Martensitic phase transformation in rapidly solidified $Mn_{50}Ni_{40}In_{10}$ alloy ribbons

J. L. Sánchez Llamazares,[a] T. Sanchez, J. D. Santos, M. J. Pérez, M. L. Sanchez, and B. Hernando
Facultad de Ciencias, Departamento de Física, Universidad de Oviedo, Calvo Sotelo s/n, 33007 Oviedo, Spain

Ll. Escoda and J. J. Suñol
Universidad de Girona, Campus de Montilivi, edifici PII. Lluís Santaló s/n, 17003 Girona, Spain

R. Varga
Institute of Physics, Faculty of Science, UPJS, Park Angelinum 9, 04154 Kosice, Slovakia

(Received 11 October 2007; accepted 1 December 2007; published online 9 January 2008)

Heusler alloy $Mn_{50}Ni_{40}In_{10}$ was produced as preferentially textured ribbon flakes by melt spinning, finding the existence of martensitic-austenic transformation with both phases exhibiting ferromagnetic ordering. A microcrystalline three-layered microstructure of ordered columnar grains grown perpendicularly to ribbon plane was formed between two thin layers of smaller grains. The characteristic temperatures of the martensitic transformation were M_S=213 K, M_f=173 K, A_S=222 K, and A_f=243 K. Austenite phase shows a cubic $L2_1$ structure (a=0.6013(3) nm at 298 K and a Curie point of 311 K), transforming into a modulated fourteen-layer modulation monoclinic martensite. © *2008 American Institute of Physics*. [DOI: 10.1063/1.2827179]

Since Sutou *et al.*[1] reported the occurrence of martensitic transformation in the ferromagnetic Heusler system $Ni_{50}Mn_{50-x}In_x$, considerable attention has been dedicated to study magnetism and magnetic shape memory effect,[2–4] magnetic entropy change,[4–8] and magnetotransport properties[9–11] of these alloys. Nevertheless, ferromagnetism in both phases is only observed in the narrow composition range of $15 \leqslant x \leqslant 16$[2]. The characteristic temperatures of the reversible first order structural transformation between both phases, referred as martensitic and austenitic starting and finish temperatures (i.e., M_S, M_f, A_S, and A_f, respectively), strongly vary upon small changes in the chemical composition. The crystal structure of austenite and martensite depends on the composition,[2,4] and the transformation can be also induced by applying a magnetic field.[2–4] Additionally, a large inverse and direct magnetocaloric effect has been measured in $Ni_{50}Mn_{34}In_{16}$.[6–8] Ni–Mn–In Heusler alloys are therefore of significant prospective importance for applications in both magnetically driven actuators due to magnetic shape memory effect and as working substances in magnetic refrigeration technology.

Until now, the investigated alloys are usually bulk polycrystals obtained by arc or induction melting followed by a high temperature annealing,[1–8,10] or single crystals grown by Czochralski method.[9,11] Present investigation was carried out to employ rapid quenching by melt spinning to produce Mn–Ni–In Heusler alloys. This technique offers two potential advantages for the fabrication of these magnetic shape memory alloys: the avoiding, or reduction, of the annealing to reach a homogeneous single phase alloy, and the synthesis of highly textured polycrystalline ribbons. Ribbon shape can be also appropriate for use in practical devices. We fabricated the alloy $Mn_{50}Ni_{40}In_{10}$ by melt spinning. Its valence electronic concentration per atom e/a is 7.801, allowing the existence of martensite-austenite transformation with both phases exhibiting ferromagnetic ordering, opening its potential use as a magnetic shape memory alloy.[3] We report in this letter a preliminary characterization of the microstructural features and magnetic behavior.

As-cast pellets of nominal composition, $Mn_{50}Ni_{40}In_{10}$ were prepared by Ar arc melting from pure elements (>99.9%). The samples were melt spun in argon atmosphere at a wheel linear speed of 48 ms^{-1}. X-ray diffraction (XRD) analyses were performed using Cu $K\alpha$ radiation (λ=1.5418 Å) with a low temperature device. Microstructure and elemental composition were examined by using a scanning electron microscope (SEM) equipped with a microanalysis system. Magnetization measurements were performed in the temperature interval of 4.2–350 K, using a physical properties measuring system (Quantum Design) platform with the vibrating sample magnetometer module. Zero-field cooling (ZFC), field cooling (FC), and field heating (FH) thermomagnetic curves were recorded at 50 Oe, and 50 kOe, with a temperature heating or cooling rate of 2 K/min. The magnetic field was applied along the ribbon axis. Curie point T_C was inferred from the minimum in the dM/dT versus T curve. Hysteresis loops were measured up to 10 kOe using a superconducting quantum interference device magnetometer.

SEM images at different magnifications of fracture cross section and the free surface of ribbons are presented in Fig. 1. As the micrographs demonstrate, the samples are fully crystalline showing fracture surfaces of a cleavage type revealing the fast crystallization and growth kinetics of the alloy. The ribbon thickness was around 7–10 μm. A thin layer of small equiaxed grains crystallizes in the ribbon surface in contact with the wheel [Fig. 1(b)]. Furthermore, an abrupt change takes place by the formation of ordered columnar grains growing perpendicularly to ribbon plane. This suggests that the rapid solidification process induces a direc-

[a]Author to whom correspondence should be addressed. Electronic mail: sanchez@nanomagnetics.org.

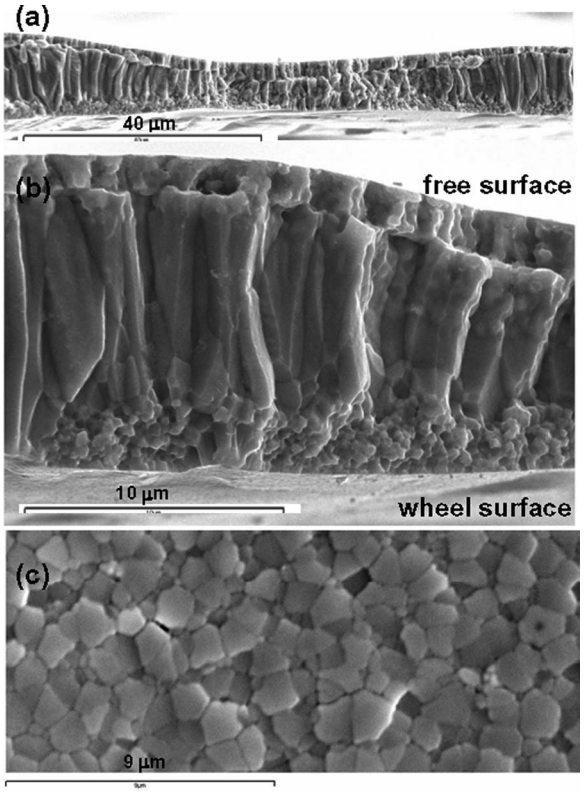

FIG. 1. SEM micrographs of the different regions of as-quenched $Mn_{50}Ni_{40}In_{10}$ ribbons: [(a) and (b)] fractured cross section at different magnification and (c) free surface.

tional crystalline grain growth. At the free surface, another thin layer of small grains appears. It cuts and covers the oriented columnar structure. The granular microstructure exhibited by the free surface is shown in Fig. 1(c).

A careful study by energy dispersive spectroscopy microanalysis was carried out to estimate the average elemental chemical composition. After numerous analyses performed on the cross section and both ribbon surfaces of different samples, we found a nearly homogeneous distribution of the chemical elements and the average composition $Mn_{49.5}Ni_{40.4}In_{10.1}$. SEM examinations in backscattering emission mode also confirmed that the chemical elements are homogeneously distributed in the alloy. Segregation of minor or secondary phases was not observed.

The ZFC, FC, and FH thermomagnetic curves recorded at 50 Oe are shown in Fig. 2. In the ZFC curve, the magnetization keeps low values and a small positive slope with the increase in temperature, and has a sudden raise at around 220 K suggesting a structural martensite-austenite phase transformation; a similar behavior is observed in the FH curve. The FC curve simultaneously confirms its reversible and thermally hysteretic character. T_C for the high-temperature austenite phase is 311 K. The characteristic temperatures of the respective martensite-austenite phase transformation are M_S=213 K, M_f=173 K, A_S=222 K, and A_f=243 K. The low-field heating and cooling $dM/dT(T)$ curves shown in the inset prove that the phase transition occurs in a broad temperature interval. As can be seen, the thermal hysteresis, estimated from the maximum in dM/dT between heating and cooling in the transition region, was as large as ΔT=38 K. The heating and cooling thermal dependences of saturation magnetization measured at a high field

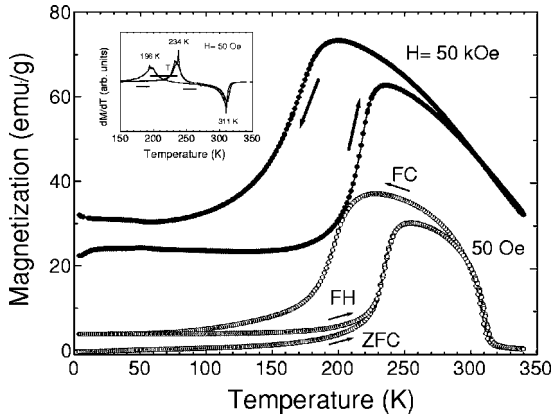

FIG. 2. Temperature dependence of the magnetization measured at H=50 Oe and H=50 kOe for as-quenched $Mn_{50}Ni_{40}In_{10}$ ribbons. The arrows indicate whether the curve corresponds to heating or cooling regimen. The inset shows the corresponding $dM/dT(T)$ curve at 50 Oe and the horizontal double arrow indicates the thermal hysteresis.

value of 50 kOe show two well distinct ferromagnetic regions and illustrates the reversible and abrupt change in M_S as well as the field dependence of the martensitic transformation. A significant decrease in the characteristic temperatures of the structural transformation is observed (estimated values: ΔM_S=−20 K, ΔM_f=−40 K, ΔA_S=−22 K, and ΔA_f=−22 K). Martensite shows a lower saturation magnetization than austenite.

The crystal structure of the formed phases was determined by recording the x-ray diffraction patterns at a temperature below and above the transformation (150 and 298 K were chosen). Diffraction patterns were recorded by exposing both ribbon surfaces to incident radiation; significant differences were not found. Diffractograms are presented in Fig. 3. At 298 K, all the Bragg peaks are sharp and were well indexed based on a bcc cubic $L2_1$-type structure with space

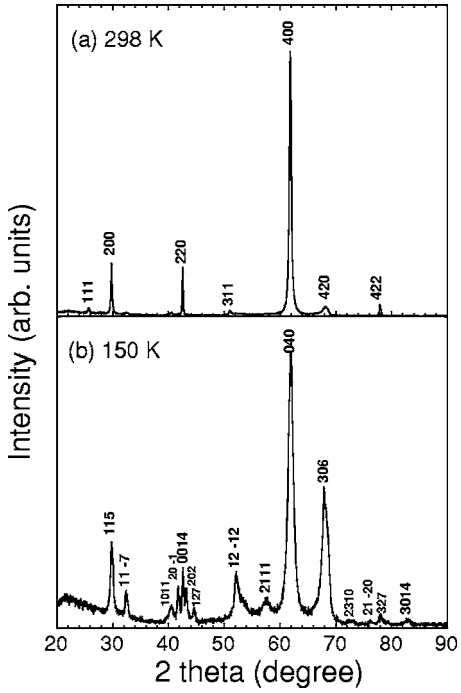

FIG. 3. X-ray diffraction patterns for as-quenched $Mn_{50}Ni_{40}In_{10}$ ribbons measured at: (a) 298 K and (b) 150 K. The crystal structures are $L2_1$ austenite and 14M monoclinic martensite, respectively.

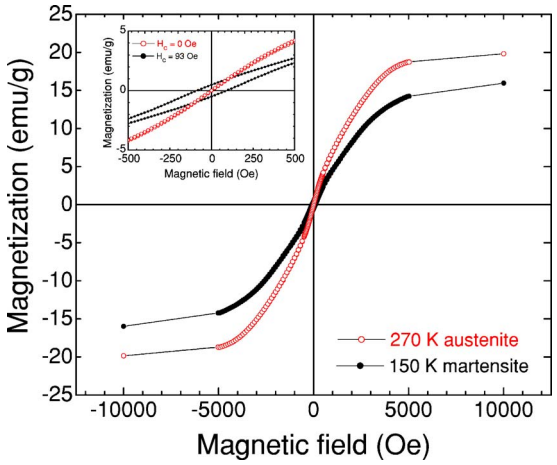

FIG. 4. (Color online) (Color online) Hysteresis loops for as-quenched $Mn_{50}Ni_{40}In_{10}$ ribbons measured at 150 and 270 K. The inset shows a zoom into the low field range.

group $Fm3m$ and a lattice parameter $a=0.6013(3)$. This reveals that ribbons are fully single phase with a cubic austenite parent phase. Below the phase transformation, the crystal structure of the martensite phase formed was identified as monoclinic with a fourteen-layer modulation (14M) and lattice parameters $a=0.4281$ nm, $b=0.5789$ nm, $c=2.966$ nm, and $\beta=93.84°$. From XRD patterns, it is also established that ribbons exhibit crystallographic texture in agreement with their grain-oriented columnar microstructure. The crystal directions [400] and [040] are preferentially oriented perpendicular to the ribbon plane at 298 and 150 K, respectively.

Hysteresis loops measured at 270 and 150 K (Fig. 4) confirm the ferromagnetic ordering exhibited by both phases. Saturation magnetization is higher for austenite phase as was previously seen from thermomagnetic curves of Fig. 2. $M(H)$ curve for austenite approaches to saturation at a lower field value being magnetically softer than the martensite, as a result of its higher symmetry cubic structure and hence lower magnetocrystalline anisotropy. The inset of Fig. 4 zooms into the low magnetic field region. Coercive field H_C for austenite is negligible within the uncertainty of the measurement (±2 Oe), while H_C for martensite is 93 Oe.

In conclusion, rapid solidification by melt spinning is an effective preparation route to obtain, in a single-step process, ribbons of the $Mn_{50}Ni_{40}In_{10}$ alloy with an homogenous chemical composition, preferential texture, and a single cubic $L2_1$ austenite phase at room temperature. As-quenched ribbons exhibit a three-layered microcrystalline microstructure. At low temperature, austenite transforms into a fourteen-layered monoclinic martensite with martensite-austenite phase transformation temperatures $M_S=213$ K, $M_f=173$ K, $A_S=222$ K, and $A_f=243$ K. Further studies are in course for understanding the role of the different factors affecting the manufacture of this Heusler alloy as melt spun ribbon with optimal textured microstructure and magneto-structural behavior, which may be a subject of significant scientific and technological interests.

FICYT is acknowledged by J.L. Sánchez Llamazares (contract No. COF07-013) and T. Sánchez for her Ph.D. grant. This work has been supported by the Spanish MEC under Project Nos. MAT2006-13925-C02-01, MAT2006-13925-C02-02, and NAN-2004-09203-C04-C03. Authors are grateful to Professor V. Shavrov, Dr. V. Koledov, and Dr. V.V. Khovaylo for helpful discussion.

[1]Y. Sutou, Y. Imano, N. Koeda, T. Omori, R. Kainuma, K. Ishida, and K. Oikawa, Appl. Phys. Lett. **85**, 4358 (2004).
[2]T. Krenke, M. Acet, E. F. Wassermann, X. Moya, L. Mañosa, and A. Planes, Phys. Rev. B **73**, 174413 (2006).
[3]K. Oikawa, W. Ito, Y. Imano, R. Kainuma, Y. Sutuo, K. Ishida, S. Okamoto, O. Kitakami, and T. Kanomata, Appl. Phys. Lett. **88**, 122507 (2006).
[4]T. Krenke, E. Duman, M. Acet, E. F. Wassermann, X. Moya, L. Mañosa, A. Planes, E. Suard, and B. Ouladdiaf, Phys. Rev. B **75**, 104414 (2007).
[5]Z. D. Han, D. H. Wang, C. L. Zhang, S. L. Tang, B. X. Gu, and Y. W. Du, Appl. Phys. Lett. **89**, 182507 (2006).
[6]X. Moya, L. Mañosa, A. Planes, S. Askoy, M. Acet, E. F. Wassermann, and T. Krenke, Phys. Rev. B **75**, 184412 (2007).
[7]V. K. Sharma, M. K. Chattopadhyay, and S. B. Roy, J. Phys. D **40**, 1869 (2007).
[8]A. Kumar Pathak, M. Khan, I. Dubenko, S. Stadler, and N. Ali, Appl. Phys. Lett. **90**, 262504 (2007).
[9]S. Y. Yu, Z. H. Liu, G. D. Liu, J. L. Cheng, Z. X. Cao, G. H. Wu, B. Zhang, and X. X. Zhang, Appl. Phys. Lett. **89**, 162503 (2006).
[10]V. K. Sharma, M. K. Chattopadhyay, K. H. B. Shaeb, A. Chouhan, and S. B. Roy, Appl. Phys. Lett. **89**, 222509 (2006).
[11]B. Zhang, X. X. Zhang, S. Y. Yu, J. L. Cheng, Z. X. Cao, and G. H. Wu, Appl. Phys. Lett. **91**, 012510 (2007).